Pergamon

Carbon Vol. 36, Nos. 1–2, pp. 123–131, 1998

0008-6223/97 $17.00 + 0.00

PII: S0008-6223(97)00169-3

EFFECT OF PORE SIZE ON ADSORPTION OF HYDROCARBONS IN PHENOLIC-BASED ACTIVATED CARBON FIBERS

C. L. MANGUN,[a,*] M. A. DALEY,[a] R. D. BRAATZ[b] and J. ECONOMY[a]
[a]Department of Materials Science and Engineering, 1304 West Green Street, Urbana, IL 61801, U.S.A.
[b]Department of Chemical Engineering, 600 South Mathews, Urbana, IL 61801, U.S.A.

(*Received* 12 *June* 1997; *accepted in revised form* 28 *July* 1997)

Abstract—The combined effect of pore size and pore volume on the equilibrium adsorption capacity and the adsorption kinetics for a series of normal alkanes is determined. The selected adsorbents, activated carbon fibers (ACFs) and air activated phenolic fibers (AAPFs), possess a range of micropore sizes and have been thoroughly characterized in past work. For the normal alkane series, the lower surface area (smaller pore size) adsorbents demonstrate higher adsorption capacities for low boiling point alkanes and for adsorbing molecules at low concentrations. For higher boiling point alkanes and at higher concentrations, the adsorption capacity is greater for higher surface area materials (larger pore size) due to increasing pore volumes.

This data was modeled using the DR equation to develop a predictive capability for adsorption based on boiling point and micropore size. For the full range of gas concentrations, the average initial mass rates of adsorption increase as the average pore size increases. © 1997 Elsevier Science Ltd

Key Words—A. Activated carbon, A. carbon fibers, B. activation, C. adsorption, D. microporosity.

1. INTRODUCTION

Growing concern over contamination of the environment has forced industry to develop responsible and effective methods for controlling the release of toxic contaminants in air and water. Adsorption of these contaminants onto an adsorbent and subsequent desorption for collection/reuse or destruction has been a primary route for purifying polluted air and water streams. Activated carbons, primarily because of their low cost, are still the most widely used material for adsorption of these impurities. One major concern in designing activated carbons for adsorption processes is that very little is reported about their structure including pore size and shape, pore volume, and pore surface chemistry. These fundamental features dominate the adsorption properties of the activated carbon. Thus, understanding the role that pore structure has on adsorption would allow activated carbons to be tailored for selective and/or enhanced removal of specific contaminants.

Recently a major effort has been undertaken in our group to determine the pore size, pore shape and pore surface chemistry of activated carbon fibers and to correlate this information with adsorption properties [1–5]. Other researchers have examined the pore size and shape indirectly by means of the application of adsorption theory to an isotherm [6,7], use of molecular probes of differing size and shape [8], application of theory to X-ray [9] and neutron scattering experiments [10], transmission electron microscopy [11], and more directly using scanning tunneling microscopy [12,13]. The pore surface chemistry has been analyzed using a variety of techniques including titration and exchange [14], diffuse reflectance infrared Fourier transform spectroscopy [15] and X-ray photoelectron spectroscopy [16,17].

In earlier work, the pore structure of commercially prepared activated carbon fibers (ACFs) was characterized by several independent techniques [3,8,12,13]. In this paper, a series of normal alkanes is used to study the effect of adsorbent pore size/volume versus adsorbate concentration and boiling point on both equilibria and kinetic properties. The adsorption characteristics of several high surface area activated carbon fibers (ACFs) are compared with those of air activated phenolic fibers (AAPFs) which were prepared in our laboratories.

2. EXPERIMENTAL

2.1 *Measurement of adsorption isotherms*

A Coulter Omnisorb 100 (Hialeah, Florida) was used for the volumetric measurement of the nitrogen adsorption isotherm at 77 K as well as the amount of methane (with a *Po* value of 760 Torr) adsorbed at room temperature. The activated fibers were outgassed for 24 hours under vacuum at 150°C prior to testing. The adsorption experiments were performed in static mode which allowed for sufficient time to reach equilibrium. The surface areas were determined using the standard Brunauer, Emmett and Teller (BET) method applied to the nitrogen experimental

*Corresponding author. Tel: +1 217 244 2523; Fax: +1 217 333 2736; e-mail: c-mangun@uiuc.edu

adsorption isotherm over a relative pressure range of 0.01 to 0.20.

The adsorption of ethane, propane, butane, pentane or benzene in a nitrogen carrier gas was measured thermogravimetrically using a TGA 951 (TA Instruments – New Castle Delaware) interfaced with the TA Instruments 2100 System Computer.

2.2 *Sample preparation*

The adsorbents studied included a series of ACFs which were commercially prepared by Nippon Kynol® through carbonizing and activating a phenolic fiber precursor in steam/carbon dioxide. The preparation of these systems is extensively described in the literature [18,19]. The fibers were designated ACF10, ACF15, ACF20 and ACF25 and had measured surface areas of 904, 1420, 1598 and 1978 $m^2 g^{-1}$, respectively.

To prepare the AAPFs, a 1–2 g sample of phenolic fabric (Kynol 5092) was placed into the center of a 5 cm diameter quartz tube with glass end caps which was then placed into a Lindberg tube furnace. The sample was heated in air to 450°C at a flow rate of 130 mL min^{-1} for a predetermined length of time. The air etched the phenolic fiber resulting in an increased surface area and a high oxygen content. The sample was weighed and the reaction yield was calculated based on the weight loss and the original fiber weight. Elemental analysis was performed using a model 240XA Elemental Analyzer (Control Equipment Corporation). The carbon and hydrogen content were determined directly while the oxygen content was calculated by difference. Table 1 contains the reaction yields, BET surface areas (*SA*) and elemental analysis results for different reaction times of the phenolic fibers in air at 450°C. The preparation and characterization of the AAPFs is described in more detail elsewhere [5,20].

2.3 *Determination of pore size for ACFs and AAPFs*

The pore size distributions of the ACFs were determined by application of the Dubinin–Radushkevich–Stoeckli (DRS) equation to the experimental nitrogen adsorption isotherm [7]. In previous ACF studies, this equation has shown excellent correlation when compared to direct observation of the porosity using STM [12,13].

For brevity, we describe here only how to compute the micropore volume, the adsorption energy and the similarity coefficient. The micropore volume *Wo* can be computed from the Dubinin equation applied to the experimental nitrogen isotherm at 77 K:

$$\log(W) = \log(Wo) - M \cdot \log^2(Po/P) \qquad (1)$$

where P/Po is the partial pressure of the adsorbate, and W is the amount of gas/vapor adsorbed in mL g^{-1} [7]. The micropore volume *Wo* is calculated from the intercept of a $\log(W)$ vs $\log^2(Po/P)$ plot, while the slope, M, of the best fit line is related to the adsorption energy, E, by

$$M = -2.303 \cdot (RT/E)^2 \qquad (2)$$

where R is the ideal gas constant and T is the adsorption temperature in kelvin. The similarity coefficient β is defined by

$$\beta = E/Eo \qquad (3)$$

where *Eo* is the adsorption energy for a reference vapor (typically benzene). The similarity coefficient is a powerful parameter because it provides a means to calculate the adsorption isotherm for any contaminant if the isotherm is known for the reference material. β characterizes the adsorbate–adsorbent interaction and is affected by pore size/shape and pore surface chemistry of the adsorbent as well as the adsorbate size and shape, boiling point, and chemistry.

The AAPFs used in this study were from the same lot used to characterize their pore structure in previous work [5]. The DR equation was not applicable since this was not a fully carbonized structure.

3. RESULTS/DISCUSSION

3.1 *Pore size for ACFs/AAPFs*

The nitrogen adsorption/desorption isotherms for the ACFs show a typical type I isotherm which is indicative of microporous materials (Fig. 1). The isotherms for the AAPFs do not fit into the present classifications which describe porous materials (Fig. 2) since the hysteresis loop continues over the entire concentration regime. Previously, the pore size of the AAPFs has been determined using molecular probe studies to be strictly less than 6 Å [5] thus providing the reason for this behavior. This curve would be very similar to a type I isotherm except that the small pores do not allow for complete equilibrium due to slow diffusion rates resulting in a sloping adsorption curve. However, once the nitrogen

Table 1. BET surface areas and elemental analysis for AAPFs with increasing activation time

Reaction time (min)	Yield (%)	BET *SA* ($m^2 g^{-1}$)	C (Wt%)	H (Wt%)	O (Wt%)
10	83.0	60	71.1	2.44	26.5
20	73.0	356	69.5	2.62	27.9
30	59.8	436	67.9	1.98	30.1
50	44.8	477	69.4	2.63	28.0
60	38.4	545	71.9	1.92	26.2

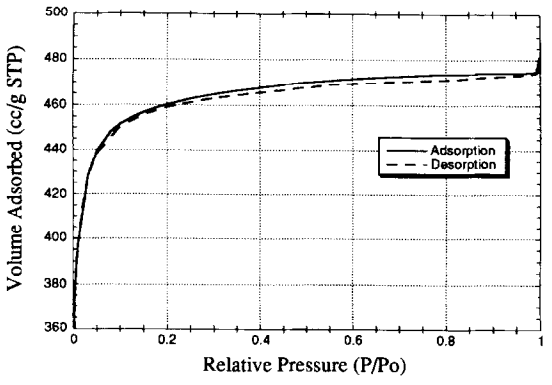

Fig. 1. Nitrogen adsorption/desorption isotherm at 77 K for ACF15.

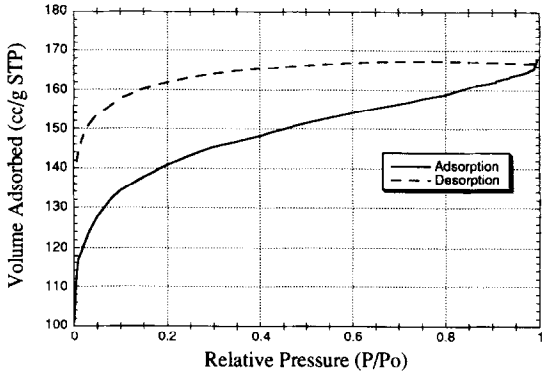

Fig. 2. Nitrogen adsorption/desorption isotherm at 77 K for AAPF with SA of 545 $m^2 g^{-1}$.

molecule is adsorbed, it remains tightly bound in the pores thus giving rise to pronounced hysteresis. Also, based on this data, the pore size for the AAPFs was shown to increase with increasing surface area. The pore size distributions for the ACFs in this study were determined by application of the DRS equation to the experimental nitrogen adsorption isotherm (see Fig. 3). As seen from the data, the average pore diameter x increases and the pore size distribution broadens with increasing surface area. The parameters used to calculate the pore size distributions are

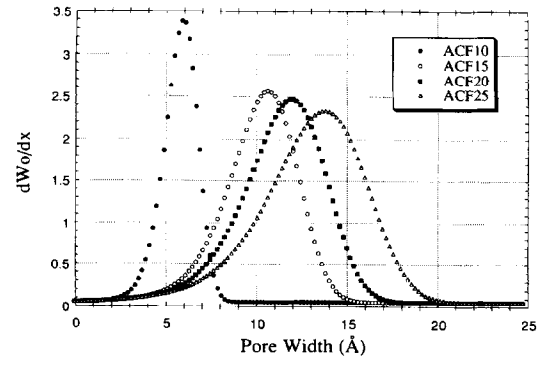

Fig. 3. Micropore size distributions for the ACFs as calculated using the DRS equation.

Table 2. Parameters used to calculate pore size distributions for ACFs

Sample	Wo (mL g^{-1})	β	E (kJ mol^{-1})	x (Å)
ACF10	0.392	0.289	9.565	6.0
ACF15	0.605	0.322	7.447	10.5
ACF20	0.679	0.332	7.009	11.7
ACF25	0.793	0.311	5.831	13.4

summarized in Table 2. The determination of these values and application of this theory to experimental data is found in the literature and will not be discussed further in this paper [5–7,13].

3.2 *Equilibrium adsorption of alkanes by ACFs*

Foster [3] showed a cross-over regime for the adsorption of butane where lower surface area (smaller pore size) ACFs adsorb better at low concentrations. This is due to a higher overlap in potential between the pore walls which binds the adsorbate more tightly and allows for the condensation of the butane molecule. As the concentration is increased, the higher surface area ACFs (larger pore size) have higher adsorption capacities due to a larger pore volume. ACF10 would adsorb better over all concentration regimes if it had the same pore volume as ACF25. However, it is difficult to produce materials of this nature since micropores tend to widen at the expense of smaller pores with increasing activation. Foster's work has been repeated with this group of ACFs (see Fig. 4). A cross-over regime was observed over a concentration range of $\sim 2 \times 10^2$ to 10^4 ppmv.

The adsorption isotherms were then measured for a normal alkane series (methane, ethane, propane and pentane) to determine how the cross-over regime shifted with boiling point (see Figs 5–8). For methane (see Fig. 5), ACF10 adsorbs better over all concentrations and no cross-over regime is observed between any of the fibers. Since methane is a small molecule with a low boiling point, it is not condensing in the pores thus making pore size the critical factor for increasing adsorption capacity. The ACF10 adsorbs

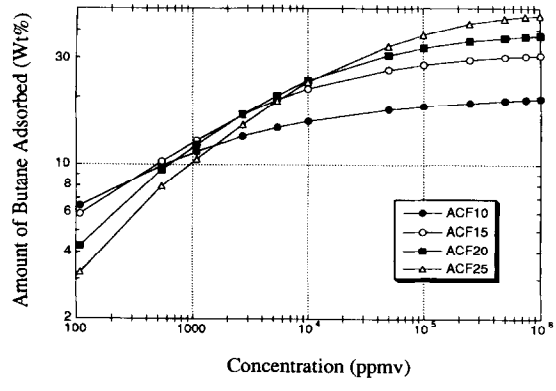

Fig. 4. The adsorption of butane at 25°C for the ACFs. A cross-over regime is observed from 10^2 to 10^4 ppmv.

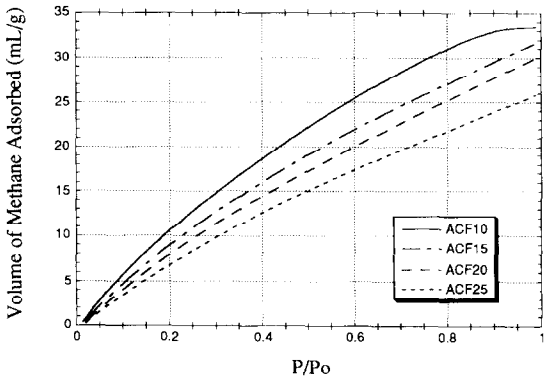

Fig. 5. The adsorption of methane versus partial pressure at 25°C for the ACFs (no cross-over is observed).

more than the other fibers because it has a larger volume of pores with small diameter. The total micropore volume is not important since only a small fraction of the pores are actually occupied. For ethane (see Fig. 6), a cross-over regime is observed from $\sim 4 \times 10^4$ to 10^6 ppmv where at lower concentrations the ACF10 (smallest pore size) adsorbs the most and the ACF25 (largest pore size) has a higher adsorption capacity at higher concentrations. For propane (see Fig. 7), the cross-over regime has now shifted down to a concentration range from $\sim 5 \times 10^3$ to 10^5 ppmv. Finally, for the highest boiling point alkane pentane (see Fig. 8), a cross-over regime is observed from 20 to 10^3 ppmv. As the boiling point of the alkane increases the cross-over regime shifts to lower concentrations.

For low boiling point alkanes, the molecule probably does not condense in the pore but rather exists as a tightly bound gas molecule, thus optimization of pore size is critical for increasing adsorption. For this adsorption to occur, the molecule must diffuse into a small pore where a high overlap in potential between the pore walls can bind the molecule. In pores of larger diameter, the overlap in potential is too weak to sufficiently hold onto the adsorbate molecule. Therefore, the amount of low boiling point alkane adsorbed increases with decreasing pore size (increasing volume of small-diameter pores). For higher boiling point alkanes, the adsorbates would prefer to condense in the pore than to remain in the vapor phase as shown by an increased adsorption capacity. But at sufficiently low concentrations, a tendency also exists for the adsorbate to remain in the vapor phase. Therefore, for high boiling point alkanes at low adsorbate concentrations, one observes a pore size/pore volume effect where both factors must be considered to optimize the adsorbents performance.

Figure 9 shows how the amount of alkane adsorbed under saturated conditions is related to the boiling point. For all alkane boiling points above -130°C, the amount adsorbed increases with increasing pore size. At alkane boiling points less than -150°C, the trend is reversed. For alkanes with higher boiling points, one notes that the ACF10 has reached an adsorption plateau indicating that its pores are filled. The other ACFs continue to increase in adsorption capacity thus all of their pore volume has not yet been utilized. Therefore, for higher boiling point alkanes under saturated conditions, optimum adsorption is attained using ACFs with larger pore size and pore volume since a higher driving force exists to condense from the gas phase in the pore due to the

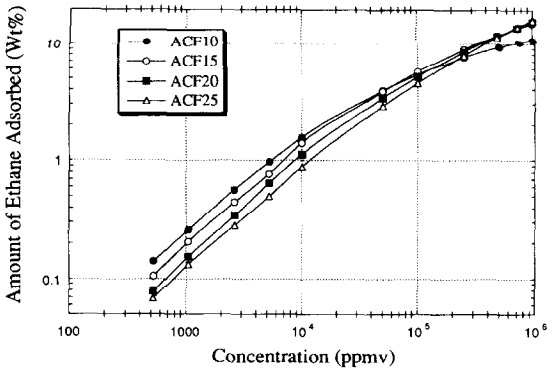

Fig. 6. The adsorption of ethane at 25°C for the ACFs. A cross-over regime is observed from 4×10^4 to 10^6 ppmv.

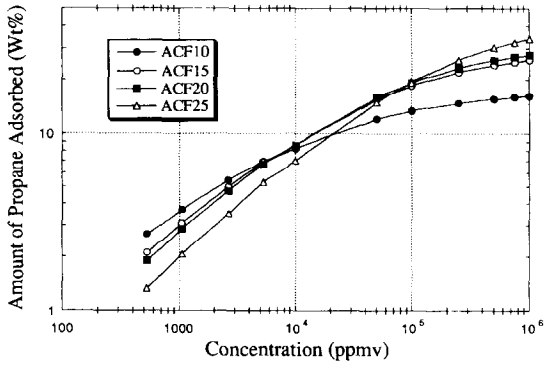

Fig. 7. The adsorption of propane at 25°C for the ACFs. A cross-over regime is observed from 5×10^3 to 10^5 ppmv.

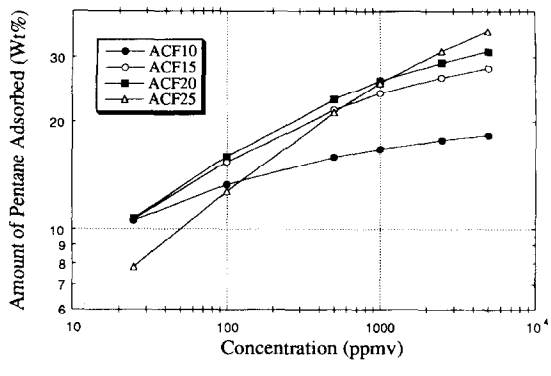

Fig. 8. The adsorption of pentane at 25°C for the ACFs. A cross-over regime is observed from 20 to 10^3 ppmv.

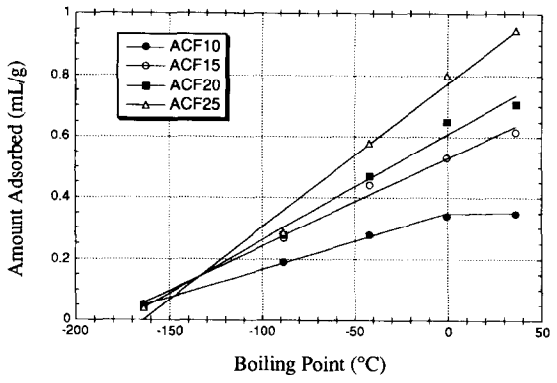

Fig. 9. The amount of alkane adsorbed versus boiling point for the ACFs under saturated conditions.

large number of species in the gas phase. For very low boiling point gases, below −150°C, the lower surface area ACFs have a higher adsorption capacity because they contain small-diameter pores which bind the adsorbate more tightly than larger pores.

3.3 *Equilibrium adsorption of alkanes by AAPFs*

The equilibrium adsorption of alkanes was also determined using the AAPFs (see Figs 10 and 11). For methane, a cross-over regime ranges between

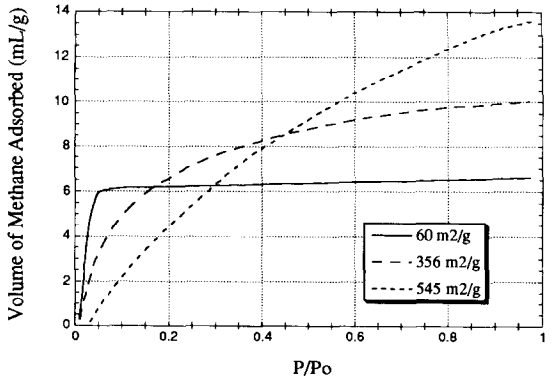

Fig. 10. The volume of methane adsorbed versus partial pressure for the AAPFs.

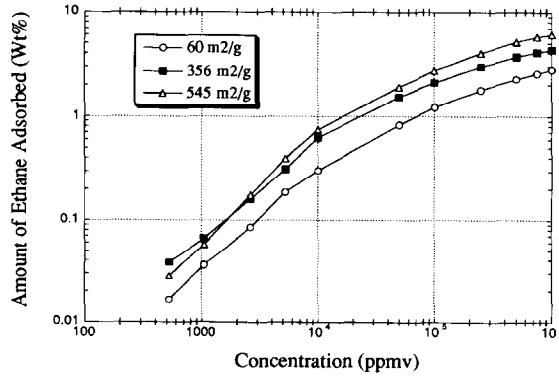

Fig. 11. The amount of ethane adsorbed versus concentration for the AAPFs.

0.15 and 0.45 *P/Po*. The lower surface area AAPF adsorbs more methane at lower partial pressures than the other AAPFs. This cross-over regime occurs for the same reasons as observed with the ACFs. For ethane, a cross-over point for the AAPFs with 356 and 545 $m^2 g^{-1}$ occurs at a concentration slightly below 2000 ppmv. No cross-over regime is seen for the AAPF with 60 $m^2 g^{-1}$ since its pore volume is too small (compared to the other AAPFs) for a molecule the size of ethane. Similarly, no cross-over regimes are observed for the larger alkanes over this concentration range (figures not shown). Due to the small pore size of the AAPFs, they are especially useful for adsorbing contaminants with low boiling points or at very low concentrations. The smaller pore size of the AAPFs (<6 Å) compared to the ACFs (see Table 2) permits enhanced adsorption (e.g. compare Figs 5 and 10 for partial pressures less than 0.1) due to a higher overlap in potential between the walls of the smaller-diameter pores.

3.4 *Relationship of β to boiling point*

For each of the alkanes and benzene, the adsorption energy was computed from the adsorption isotherms as described in Section 2.3 (see Table 3). The corresponding similarity coefficients β were then computed from eqn (3). The adsorption energy increases with decreasing pore size because of the higher overlap in potential between the pore walls. The adsorption energy also increases with increasing boiling point of the alkane because a less volatile adsorbate has a stronger preference for condensing as a liquid in the pores.

The similarity coefficient β increases exponentially with boiling point for the ACFs (see Fig. 12). For each adsorbent, the adsorption isotherm can be predicted using *Eo* (in Table 3), the boiling point of the alkane and the temperature *T*. To do this, the similarity coefficient β is read from Fig. 12, and used with *Eo* to compute the adsorption energy *E* from eqn (3). *M* may be computed from the temperature *T* and the adsorption energy *E* using eqn (2), and the adsorption isotherm may be determined using the following rearrangement of eqn (1):

$$\log(W/Wo) = -M \cdot \log^2(Po/P) \qquad (4)$$

For ACFs with pore sizes intermediate to the ACFs studied, the adsorption isotherm can be predicted using Fig. 13. To do this, read the fitting coefficients *A* and α from Fig. 13, calculate the similarity coefficient β from the equation in Fig. 12, and then repeat the aforementioned procedure.

3.5 *Adsorption kinetics of butane for ACFs*

Uptake curves were measured for each of the ACFs for several of the alkanes at different steady-state gas concentrations. Representative curves are shown in Figs 14 and 15 at butane concentrations of 542 ppmv and saturated conditions, respectively. Since the concentration dependence of the micropore

Table 3. Energies of adsorption, E (kJ mol^{-1}), as calculated from experimental adsorption isotherms for the ACFs using the DR equation

Fiber type	Methane	Ethane	Propane	Butane	Pentane	*Eo* (Benzene)
ACF10	5.45	9.31	14.03	21.61	32.93	33.13
ACF15	5.21	8.93	12.09	17.48	24.11	23.16
ACF20	5.02	8.72	11.71	15.31	22.86	21.14
ACF25	4.83	8.73	10.91	14.00	18.48	18.75

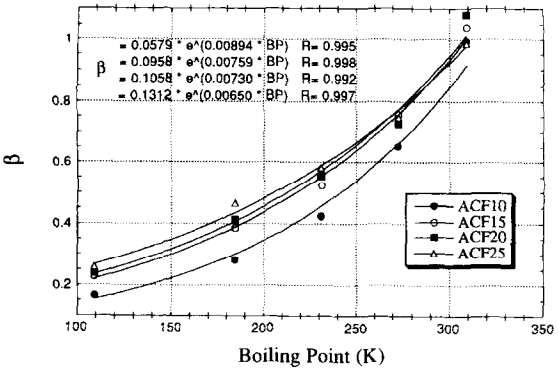

Fig. 12. The β parameter versus alkane boiling point for the ACFs ($\beta = A \cdot e^{x \cdot BP}$).

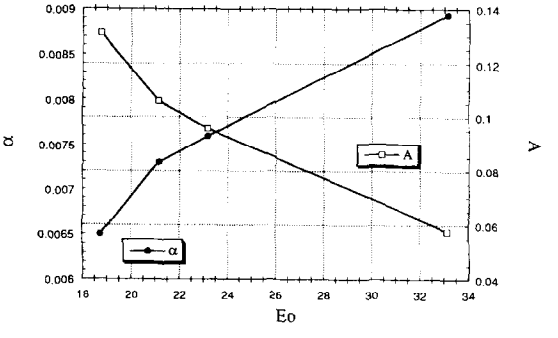

Fig. 13. The exponential fitting parameters from Fig. 12 versus *Eo*.

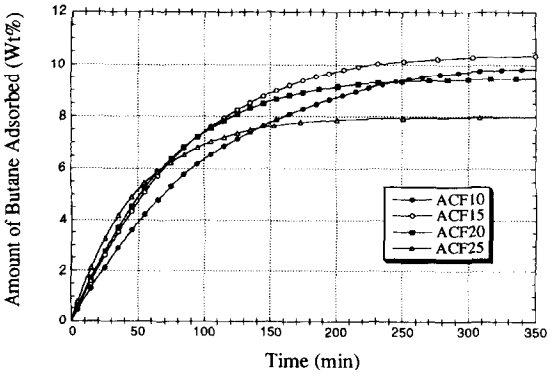

Fig. 14. The amount of butane adsorbed with time for the ACFs at a concentration of 542 ppmv.

diffusivities was not of interest here, the ACFs were characterized using concentration-averaged diffusion coefficients [21–23]. The average diffusion coefficients

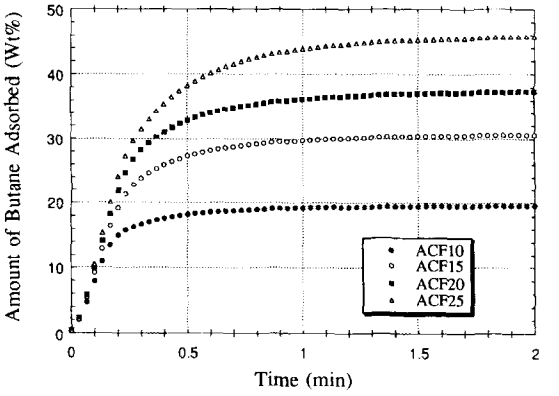

Fig. 15. The amount of butane adsorbed with time for the ACFs under saturated conditions.

listed in Table 4 provide the optimal least squares fit between an experimental uptake curve (in either Figs 14 or 15) and the theoretical uptake curve (Equation 5.23 of Crank [23]). The 95% confidence intervals were computed using standard statistical techniques (Equations 7.7.2 and 7.7.7 of Beck and Arnold [24]). The average diffusion coefficients are two orders-of-magnitude larger for saturated than for 542 ppmv butane gas concentration. The average diffusion coefficients for saturated butane gas concentration decrease as the average pore size increases, whereas the diffusion coefficients for 542 ppmv butane gas concentration do not show a clear trend. Under saturated conditions, the pores are presumably filling by a capillary condensation process which would result in the smaller pores having a higher diffusivity. The diffusivity at lower concentrations is based on both the diffusion into the fiber and the probability of the adsorbate molecule finding an adsorption site. These competing effects are difficult to separate therefore the data was analyzed in a more practical manner.

Probably more important in judging the suitability of a particular adsorbent is its rate of adsorption as a function of total mass transfer. For the ACFs, the average initial mass rate of adsorption increases as the average pore size increases (and the pore size distribution broadens). This trend was observed for all the alkanes over the entire range of gas concentrations (adsorption curves other than Figs 14 and 15 not shown for brevity). At high gas concentrations, adsorption can take place at more adsorption sites in ACFs with larger pore sizes (see Section 3.3),

Table 4. Concentration-averaged diffusion coefficients (D) and average initial adsorption rates for butane at saturated and 542 ppmv conditions

Fiber type	D (sat) ($m^2 s^{-1} \times 10^{-13}$)	D (542 ppmv) ($m^2 s^{-1} \times 10^{-15}$)	Average rate (sat) first 20 s (wt% min^{-1})	Average rate (542 ppmv) first 30 min (wt% min^{-1})
ACF10	8.7 ± 0.5	1.25 ± 0.04	79	0.078
ACF15	5.3 ± 0.3	1.31 ± 0.04	106	0.094
ACF20	4.4 ± 0.2	1.42 ± 0.04	123	0.098
ACF25	2.5 ± 0.1	1.30 ± 0.04	136	0.104

leading to a higher average initial mass rate of adsorption although the diffusion coefficients are reduced. At low butane gas concentrations, the smaller radii of the fibers (and hence increased external surface area per unit mass fiber) in ACFs with larger pore sizes result in higher average initial mass rates of adsorption.

4. CONCLUSIONS

To successfully design adsorbents, it is necessary to have a full understanding of the adsorbent structure including pore size/shape as well as the adsorbate properties. For ACFs and AAPFs, it was shown that:

For the normal alkane series, the lower surface area (smaller pore size) materials had higher adsorption capacities for low boiling point gases/vapors and for adsorbing contaminants at low concentrations. For higher boiling point gases/vapors and for adsorbing contaminants at higher concentrations, the adsorption capacity was higher for higher surface area materials (larger pore size) due to larger pore volumes. This resulted in cross-over regimes that shifted from higher concentrations to lower concentrations with increasing boiling point. The cross-over regime occurs due to a pore size–pore volume effect where at lower concentration the smaller pores fibers have a higher overlap in potential which binds the adsorbates molecule more tightly. At higher concentrations, the larger pore volumes are utilized and therefore the adsorption capacities are higher.

For the full range of gas concentrations, the average initial mass rates of adsorption increase as the average pore size increases. At high gas concentrations, adsorption can take place at more adsorption sites in ACFs with larger pore size, leading to a higher average initial mass rate of adsorption although the average diffusion coefficients are reduced. At low gas concentrations, the smaller radii of the fibers in ACFs with larger pore sizes result in higher average initial mass rates of adsorption.

The similarity coefficient β was related to the micropore structure for this series of activated carbon fibers. A method was devised to determine isotherms for different adsorbates by running only one isotherm with the reference vapor and knowing the boiling point of the adsorbate of interest.

REFERENCES

1. Economy, J., Foster, K. L., Andreopoulos, A. G. and Jung, H., *CHEMTECH*, 1992, **22**(10), 597.
2. Mangun, C. L., Daley, M. A. and Economy, J., *Proceedings of the 88th Annual Meeting of Air and Waste Management Association*, San Antonio, TX, 1995.
3. Foster, K. L., Fuerman, R. G., Economy, J., Larson, S. M. and Rood, M. J., *Chem. Mater.*, 1992, **4**(5), 1068.
4. Daley, M. A., Mangun, C. L., Debarr, J. A., Riha, S., Lizzio, A. A., Donnals, G. L. and Economy, J., *Carbon*, 1997, **35**(3), 411.
5. Daley, M. A., The development and characterization of tailored, high surface area adsorbents for enhanced adsorption. Ph.D. thesis, University of Illinois, Urbana, IL, 1996.
6. Marsh, H. and Rand, B., *J. Colloid Interface Sci.*, 1970, **33**(1), 101.
7. Dubinin, M. M. and Stoeckli, H. F., *J. Colloid Interface Sci.*, 1980, **75**(1), 34.
8. Kasaoka, S., Sakata, Y., Tanaka, E. and Naitoh, R., *Int. Chem. Eng.*, 1989, **29**(4), 734.
9. Dubinin, M. M., Plavnik, G. M. and Zaverina, E. D., *Carbon*, 1964, **2**(3), 261.
10. Kieffer, J., *J. Appl. Phys.*, 1992, **72**, 12.
11. Marsh, H., Crawford, D., O'Grady, T. M. and Wennerberg, A., *Carbon*, 1982, **20**(5), 419.
12. Economy, J., Daley, M. A., Hippo, E. and Tandon, D., *Carbon*, 1995, **33**(3), 344.
13. Daley, M. A., Tandon, D., Economy, J. and Hippo, E., *Carbon*, 1996, **34**(10), 1191.
14. Barton, S. S., Dacey, J. R. and Evans, M. J. B., *Colloid Polym. Sci.*, 1982, **260**(7), 726.
15. Ermolenko, I. N., Lyubliner, I. P. and Gulko, N. V., *Chemically Modified Carbon Fibers*. Academy of Sciences, Minsk, U.S.S.R., 1990.
16. Desimoni, E., Casella, G. I., Morone, A. and Salvi, A. M., *Surf. Interface Analysis*, 1990, **15**, 627.
17. Proctor, A. and Sherwood, P. M. A., *Surf. Interface Analysis*, 1982, **4**(5), 212.
18. Lin, R. Y. and Economy, J., *Appl. Polym. Sym.*, 1973, **21**, 143.
19. Economy, J. and Lin, R. Y., *Appl. Polym. Sym.*, 1976, **29**, 199.
20. Andreopoulos, A. G. and Economy, J., *Chem. Mater.*, 1991, **3**(4), 594.
21. Cunningham, R. E. and Williams, R. J., *Diffusion in Gases and Porous Media*. Plenum Press, New York, 1980.
22. Ruthven, D. M., *Principles of Adsorption and Adsorption Processes*. Wiley, New York, 1984.
23. Crank, J., *The Mathematics of Diffusion*, 2nd edn. Oxford University Press, New York, 1995.
24. Beck, J. V. and Arnold, T. J., *Parameter Estimation in Engineering and Science*. Wiley, New York, 1977.